2024 IEEE International Conference on Robotics and Automation (ICRA 2024)
May 13-17, 2024. Yokohama, Japan

Non-Intrusive LiDAR Protection Module Emulating Bio-Inspired Wiping Motion for Outdoor Unmanned Vehicles

Youngrae Kim[1], Seunghyun Lim[1], Lee Hanmin[2], Seokchan Kim[2], Ji-Chul Kim[2,†], and Dongwon Yun[1,†]

***Abstract*— In this paper, we have developed a protection module for Light Detection and Ranging (LiDAR) sensors used in outdoor unmanned vehicles. Bio-inspired wiping motion was figured to have more efficient and excellent wiping performance than conventional cleaning methods for LiDAR sensors. An water wiping experiment confirmed that the finger wiping motion removed 35% more water than the translational wiping motion. Also, the theoretical analysis for the existence of an optimal rotational speed at maximum wiping performance was verified to be consistent with the experiment. The LiDAR distortion experiment results demonstrated no data distortion, showing an average error of up to 0.40% for detecting obstacles even when the acrylic cover rotates. Finally, a contamination protection experiment was conducted for water, powder, soil, and mud. As a result, although there was a change in the number of pointcloud and a decrease in the intensity of the sensor data after contamination, it was validated that the number of pointclouds and average intensity of data could be restored to at least 97% and 67% after being cleaned.**

I. INTRODUCTION

Robots such as wheel-based robots [1], [2], [3], walking robots [4], [5], [6], and drones [7], [8], [9] use Light Detection and Ranging (LiDAR) sensors to quickly and accurately understand the surrounding environments for autonomous driving in outdoor environments. In these cases, the LiDAR sensor may be contaminated and damaged due to external environmental factors such as rain, snow, dust, mud, and stones. Since the objects are measured through light, such contamination and damage significantly impact the detection performance of the LiDAR sensor [10], [11], [12]. Therefore, outdoor environment sensors must be equipped with protection and cleaning devices. For the regular operation of vehicles, various cleaning technologies were applied to cameras [13], [14], and Waymo [15] applied cleaning technologies to LiDAR sensors as well.

There are two representative protection technologies. The first is a non-contact method that removes contaminants by protective coating on the cover or spraying air and liquid at high pressure. Protective coatings can prevent most liquids from being contaminated [16], but do not remove sticky dusty contaminants. Cleaning the sensor by spraying compressed air at high pressure is effective [17], but the protector's surface may fog up, and old contaminants may not be cleaned. For this reason, research on cleaning by spraying water or cleaning liquid was also conducted [18]. However, this method has the disadvantage of requiring additional water tanks, and the sprayed liquid may remain on the protector's surface.

Fig. 1. LiDAR protection module for outdoor unmanned vehicles.

The second is the contact cleaning method, which removes contaminants directly through a wiper. The vehicles such as cars and airplanes are already widely used wipers. However, in dry environments, it may cause permanent damage to the surface of the sensor protector [19], [20] and must be used with a cleaning liquid. Because the wiper is a device that pushes contaminants vertically or horizontally, there is a high possibility that contaminants will remain. Thus, this translational wiping motion is inefficient in terms of energy because it must be repeatedly operated until the contaminants are completely removed.

In this paper, we emulated the motion of human fingers wiping away contaminants to develop a LiDAR sensor protection module(Fig. 1). In section II, it was proven through theoretical analysis and experiment that the proposed human finger wiping motion showed excellent cleaning performance with high efficiency. Section III deals with the hardware development of the protection module applying the finger motion. Lastly, section IV experimentally verified that the fabricated sensor protection module does not distort sensor data and shows excellent cleaning performance even in various contaminated environments.

This work was supported by the National Research Foundation of Korea (NRF) grant funded by the Korea government (MSIT) (No. 2020R1C1C1012279). And this research was supported by a grant of the Basic Research Program funded by the Korea Institute of Machinery and Materials (grant number : NK242I). *(†Corresponding author: Ji-Chul Kim and Dongwon Yun.)*

[1]Authors are with the Department of Robotics and Mechatronics Engineering, Daegu Gyeongbuk Institute of Science and Technology (DGIST), Daegu, 42988 South Korea (email: wutzahaha@dgist.ac.kr; shl0216@dgist.ac.kr; mech@dgist.ac.kr)

[2]Authors are with the Department of Smart Industrial Machine Technologies, Korea Institute of Machinery and Materials (KIMM), Daejeon, 34103 South Korea (email: hmlee@kimm.re.kr; chan@kimm.re.kr; jckim@kimm.re.kr)

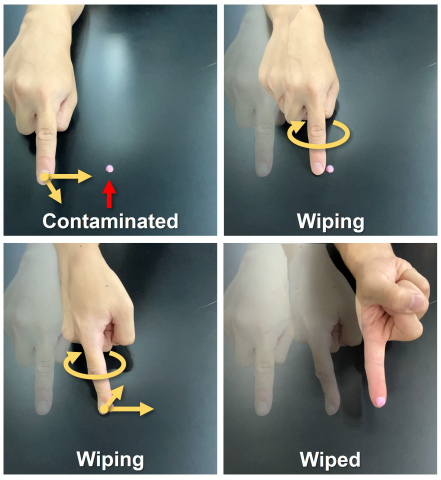

Fig. 2. Human finger wiping motion for the contamination.

II. BIO-INSPIRED WIPING MOTION

A. Human Finger Wiping Motion

When a contaminant adheres to one's clothes or objects, humans use their thumb, index finger, or middle finger to remove it. This operation consists of the sequence of Fig. 2. First, the finger is placed near the contaminants on the object, and force is applied to the finger to increase the pressure on the contact surface and expand the surface area. Finally, it generates translational and rotational movements in the fingers simultaneously. This way, contaminants such as water, dust, and sauce attached to the object are removed by moving them to fingers. The conventional cleaning methods of LiDAR sensors are inefficient because they require additional water tanks or several repetitive movements. On the other hand, by emulating human finger wiping motion, it is expected that it will be possible to remove contaminants with just a single movement.

B. Water Wiping Analysis

Water plays an essential role in the interaction of fingers with objects [21], [22]. The action of wiping water with a finger can be depicted in Fig. 3(a). First, fingers touched the parallel plate and then moved it near the water. To prevent water leaking between the plate and the finger, a force F_{finger} is applied to maintain pressure, and the finger moves parallel to the plate at a translational speed of v_t. If the area is enlarged near the point O where the plate, finger, and water are in contact, the contact surface between the finger and water can be seen. The arc length s and the straight length l of the contact surface are as follows.

$$s = r\alpha \tag{1}$$

$$l = 2rsin\frac{\alpha}{2} \approx r\alpha \tag{2}$$

If the amount of the water is small, the angle α becomes small and length l can be approximated to be equal to s. Thus, the contact surface between the finger and water can be approximated as flat as shown in Fig. 3(b). Assuming

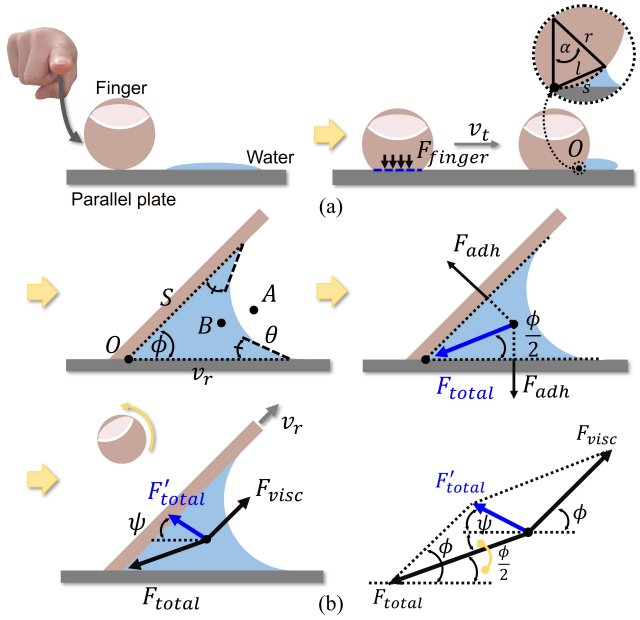

Fig. 3. Force analysis of human finger wiping motion. (a) Macro perspectives. (b) Enlarged perspectives.

the finger surface is a flat plate, the ϕ is an angle between the finger plate and the parallel plate. The adhesion force between two parallel plates in contact with water can be obtained as [23], and in this section, we extend it to the two plates forming an angle ϕ. Assuming that both plates are made of the same hydrophilic material, and that water has the same contact angle θ and contact area S with each plate. At this time, just before the finger is removed from the parallel plate is observed when $F_{finger} = 0$ and $v_t = 0$. The pressure at points A and B satisfies the equation below due to the surface tension.

$$P_A - P_B = P_{atm} - P_B = \frac{T}{R}. \tag{3}$$

P_N is the pressure at point N (P_{atm} is atmospheric pressure), T is the surface tension, and R is the radius of curvature. The force applied to the water due to the adhesion force with each plate and the magnitude of the net force of them are as follows.

$$F_{adh} = (P_A - P_B)S = \frac{TS}{R}, \tag{4}$$

$$F_{total} = 2F_{adh}sin(\frac{\phi}{2}) = \frac{2TS}{R}sin(\frac{\phi}{2}). \tag{5}$$

F_{total} forms an angle of $-\frac{\phi}{2}$ with the parallel plate, which means the water will still remain on the parallel plate. The translational wiper method is explained as a phenomenon up to this point. If the finger plate moves with only a translational speed of $-v_t$, the water cannot be wiped away from the parallel plate.

The rotational motion in finger wiping makes the plate move at a speed of v_r in the direction of an angle ϕ with the parallel plate. Then, the water receives a viscous force F_{visc} depending on the area in contact with the finger plate.

The magnitude of $F_{total}^{'}$, which is the net force of F_{total} and F_{visc}, can be obtained as the following equation.

$$F_{visc} \propto v_r, \tag{6}$$

$$F_{total}^{'} = \sqrt{{F_{visc}}^2 + {F_{total}}^2 + 2F_{visc}F_{total}cos(\pi - \frac{\phi}{2})}$$
$$= F_{visc}cos(\phi + \psi) + F_{total}cos(\frac{\phi}{2} + \psi). \tag{7}$$

F_{visc} is proportional to v_r. $F_{total}^{'}$ forms an angle of ψ with the parallel plate, and its range is $-\frac{\phi}{2} < \psi < \pi - \phi$. If the finger plate rotates at a sufficient speed v_r, ψ will have a value greater than 0, and $F_{total}^{'}$ will have the effect of wiping water from the parallel plate. The wiping effect by $F_{total}^{'}$ is greatest when $\psi = \frac{\pi}{2} - \phi$, that is, in the direction perpendicular to the finger plate and pointing to the center of rotation. And thereafter it decreases in range $\psi > \frac{\pi}{2} - \phi$. It is important to note that the wiping effect does not constantly increase as $F_{total}^{'}$ increases. As a result, the operation is interpreted to mean that there is a finite rotational speed value at which wiping performance is maximized. Additionally, if both plates are not hydrophilic, the interpretation tendency may vary. For example, if the finger plate is hydrophilic and the flat plate is hydrophobic, the adhesion force of the finger plate may increase relatively, increasing the cleaning effect.

C. Water Wiping Experiments

To verify the analysis of the finger wiping motion of water and to prove that the performance is superior to the translational wiper method, a wiping experiment device was constructed as shown in Fig. 4(a). The wiping device consists of two pairs of DC motors and controllers (Geared Encoder DC Motor and EPOS2 24/2 DCX Controller, Maxon, Switzerland), which perform torque control and velocity control for each axis. The wiping device is attached to a 3-axis linear stage. At the end of the wiping device, microfiber is attached to a cylindrical roll of deformable Thermoplastic Polyurethane (TPU). An acrylic plate was installed on the floor, water sprayed on it, and then wiping proceeded. In all cases, $1.4ml$ of water is sprayed through a syringe, and the linear stage moves at $10mm/s$. The operation consists of three steps: contact, wiping, and wiping away. Each motor's torque and velocity control graph is shown in Fig. 4(b).

The graph in Fig. 4(c) shows the amount of remaining water in percentage according to torque and rotational velocity values. It can be seen that the amount of remaining water decreases as the pressing torque increases. At $0Nm$, the contact surface area is like a line contact and water leaks out, so an average of about 69.2% of water remains, and at $0.3Nm$ and $0.6Nm$, the water is removed, so an average of about 49.7% and 17.9% are left. The most significant remaining amount in the rotational velocity was $0rpm$, the same as a translational wiper operation, and $23rpm$. It decreased to the minimum from about $7 \sim 13rpm$. The minimum value was at $0.6Nm$ and $10rpm$ with 0.1%. Considering the previous theoretical analysis, $10rpm$ means that the ψ reaches $\frac{\pi}{2} - \phi$, which shows the maximum wiping effect. In this way, it was confirmed that the finger wiping motion has excellent performance than the translational wiper motion, and the theoretical analysis that there will be a speed at which the wiping performance is maximum was experimentally verified.

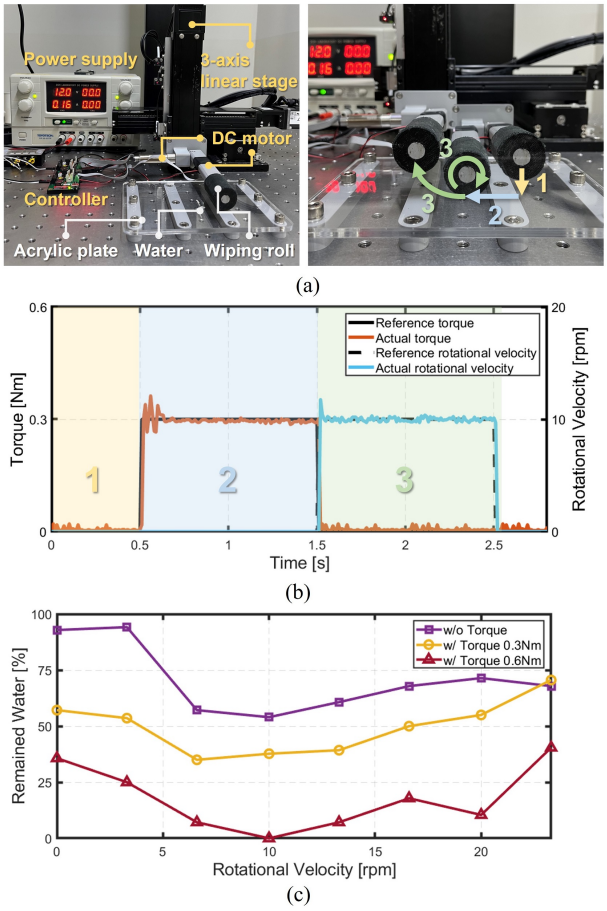

Fig. 4. Water wiping experiments. (a) Experimental setup. (b) Torque and rotational velocity control graph. (c) Water wiping performances.

D. Powder and Mixture Wiping

The principle of wiping away powdery contaminants such as sand and dust with your fingers is relatively simple. Actual fingers may have adhesion due to oil from sweat, but this is not considered in the sensor protection module being developed. If friction occurs between the finger and the contaminated object, static electricity may be generated depending on the material. At this time, contaminants such as dust can be removed from the fingers by electrostatic attraction. Additionally, fingerprints and the rough structure of the finger surface may come into contact with the particle structure of the contaminant and be removed by the physical force generated by the structure. From this perspective, fibers are materials that can play a role similar to fingers. Fibers generate static electricity relatively easily when fiction occurs. Additionally, the cross-sectional structure of the fiber

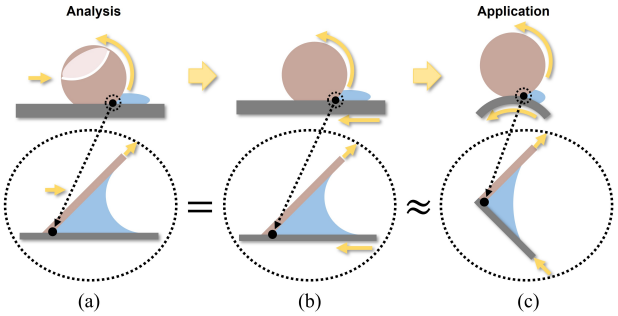

Fig. 5. Relative motion of the finger and plate and enlarged view. (a) Human finger wiping motion. (b) Relatively same motion with (a). (c) Applicated motion to the protection module.

strands is suitable for contaminants to stick. Therefore, it may be helpful to use microfiber in the same way as in the water wiping experiment above. In the case of a mixture of water, sand, and dust, it can be seen as an integration of the principles for water and the principles for powder. Additional experiments on cleaning powders and mixtures are covered in detail in Section IV.

III. LIDAR PROTECTION MODULE DESIGN

A. Protection Module and Wiping Roll Design

The human finger wiping motion consists of translational and rotational movements of the finger, and when enlarged, can be expressed as the relative motion of two flat plates as shown in Fig. 5(a). Performing both translational and rotational movements requires complex structures in hardware design. If the flat plate moves in the opposite direction as in Fig. 5(b), the same relative motion as in Fig. 5(a) is possible, and the design can also be simplified. However, the movement of such a flat plate is difficult to apply to the LiDAR protection module because of the LiDAR's cylindrical shape. Instead of a flat plate, the operation of rotating a cylindrical plate was applied to the LiDAR protection module. As explained in the previous section, as the contact surface of the finger can be approximated as a flat plate when the amount of water is small in an enlarged view, a cylindrical plate can also be approximated as a flat plate. Therefore, the method of Fig. 5(c) performs similar relative motion in Fig. 5(a), the human finger wiping analysis can be applied.

As shown in the expanded view in Fig. 6(a), the sensor protection module covers the LiDAR sensor, and a cleaning device is installed outside. The LiDAR sensor is fixed to the bottom fixture, the rotating part and the control box are fixed on it, and the cylindrical acrylic cover is attached to the rotating part. A $2mm$ thick acrylic cover protects the LiDAR sensor's sensing area, and the acrylic cover's distortion effect is covered in detail in section IV. The control box is equipped with a battery, sensor, controller, and Micro Controller Unit (MCU) to operate the module. The outer walls of the rotating part and control box are designed with an embossed structure to increase the surface area and effectively dissipate heat

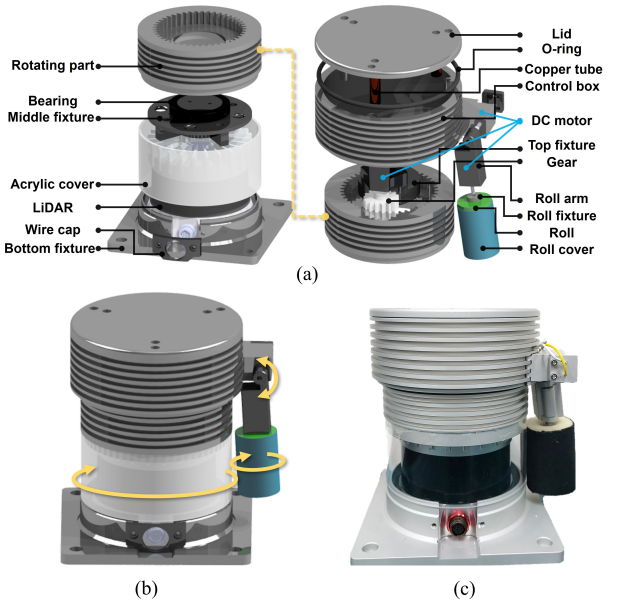

Fig. 6. LiDAR protection module design. (a) Expanded view of protection module. (b) 3D design. (c) Manufactured hardware.

generated from the LiDAR sensor. In addition, to minimize the heat transferred from the rotating part to the control box's internal parts, the rotating part and the lid are connected through a copper tube which has a high heat conductivity coefficient to allow heat to radiate upward.

The sensor protection module is driven in three Degree-of-Freedom (DOF) using three micro metal geared DC motors (Micro Metal Gearmotors, Pololu, USA). One is used to rotate the rotating part, and the other two are used to rotate the roll arm and roll. Normally, the roll arm is raised so as not to block the LiDAR. If contamination is detected, the rotating part is turned to move the contaminated area near the roll, then the roll arm is lowerd and the cover and roll are rotated together to clean it. As such, the protection module cleans contamination in a single operation, providing superior energy efficiency. The cleaning roll is fixed to the shaft of a DC motor mounted at the end of the roll arm. The innermost part of the roll contains a rigid cylindrical wick of Acrylonitrile butadiene styrene (ABS) material. A hollow cylindrical structure designed with TPU material is installed outside the wick. Because it is deformable, it expands the surface area when pressed, like a finger. Microfiber was attached to the outermost part to effectively remove water and powder and minimize damage to the surface of the acrylic cover. The final design is as shown in Fig. 6(b), and all fixed parts, rotating parts, control box, roll arm, and lid are made of aluminum, as shown in Fig. 6(c).

B. Electronics and Communication

The sensor protection module's three DOF DC motor is operated through the L9110 motor driver. The motors rotating roll and rotating part control the rotation speed through Pulse Width Modulation (PWM) control. The roll

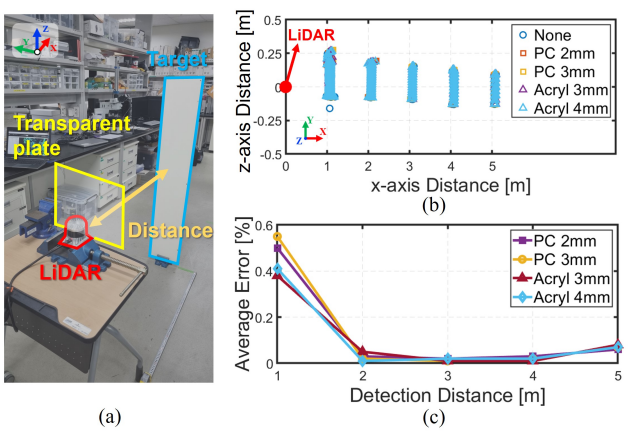

Fig. 7. Sensor data distortion tests for different materials of the plate. (a) Experimental setup. (b) Projection graph of pointcloud data. (c) Distortion performances graph.

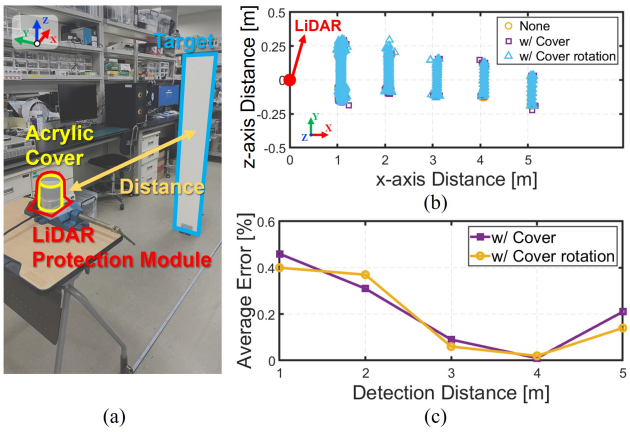

Fig. 8. Sensor data distortion tests for circular cover and its rotation. (a) Experimental setup. (b) Projection graph of pointcloud data. (c) Distortion performances graph.

arm's motor controls the current using an additional current sensor ACS712. In a non-contaminated environment, the roll arm is raised to prevent interference with the sensor area. When contamination occurs, the arm is lowered, and cleans the sensor. All sensors and drivers are connected to the Arduino Nano, an MCU. The power is supplied through a lithium-polymer battery.

To test the performance of the LiDAR sensor protection module, OS0 LiDAR sensor (OS0-32, Ouster, USA) was adopted. Data from the LiDAR sensor was acquired using the ROS package on a Laptop PC with an Ubuntu 18.04 environment. While the experiment progresses, sensor data is published as a ROS topic in PointCloud2 format and saved as a rosbag file. In the experimental analysis, information such as x, y, z, and $intensity$ was extracted and used from the data in the saved rosbag file.

IV. Experiments and Results

A. LiDAR Distortion Tests

Since the protection module covers the LiDAR sensor, it may distort the sensor data. In this section, the experimental environment was established as shown in Fig. 7(a) to quantitatively confirm the distortion effect of the transparent plate. Four types of transparent plates ($2mm$ and $3mm$ thick polycarbonate (PC), $3mm$, and $4mm$ thick acrylic) were installed in front of the sensor. The sensor acquires pointcloud data. A rectangular-shaped detecting target installed at a distance of $1 \sim 5m$ for 5 seconds. The experimental results are shown in Fig. 7(b), (c). Fig. 7(b) is a graph projecting the pointclouds of the detecting target onto the XY plane. Fig. 7(c) is the result of the average error of the detected distance compared to the with and without a transparent plate. The four types of transparent plates showed average errors within 0.55% for targets at a distance of $1m$ and within 0.08% for targets at other distances, regardless of material or thickness. In particular, acrylic showed smaller errors compared to PC. Through this, it can be confirmed that these two transparent material plates do not significantly impact the sensor's distance data and that acrylic has relatively less distortion than PC.

However, the LiDAR sensor protection module uses a rotating cylindrical-shaped cover. Therefore, it is necessary to confirm the influence of both a cylindrical acrylic cover and rotation. The experimental environment was constructed as shown in Fig. 8(a) in a similar manner to Fig. 8, and the experimental results are shown in Fig. 8(b) and (c). The fixed rectangular-shaped cover was replaced with a rotatable cylindrical acrylic cover. As a result of the experiment, the average error of the detected distance was shown to be within a maximum of 0.46% without cover rotation, and 0.40% with cover rotation. The presence of cover rotation did not significantly affect the data. Therefore, this experiment confirmed that the cover rotation did not cause significant distortion to the sensor data.

B. Contaminated Environment Protection Experiments

In this section, we designed a contaminated environment protection experiment assuming that the water, power, soil, and mud would contaminate the sensor protection module in an outdoor environment. Three types of mud were produced by mixing $20g$, $40g$, and $60g$ of soil with $100ml$ of water. The cleaning experiment was conducted by placing a rectangular-shaped detection target in front of the sensor and acquiring pointcloud data for three cases: before contamination, after contamination, and after cleaning. The results were evaluated based on how well the target was recognized.

The pointclouds were acquired for each situation as shown in Fig. 9(a), and pointclouds for the detection target were projected onto the YZ plane as shown in Fig. 9(b). Fig. 9(b) is the result of calculating the concave hull for the projected points to visually check how well the sensor detects the reference rectangular shape in each situation. If the sensor is contaminated, it may not maintain the reference shape. But, it can be seen that it returns to a reference shape after cleaning. The results of the quantitative analysis of cleaning performance are shown in Table I.

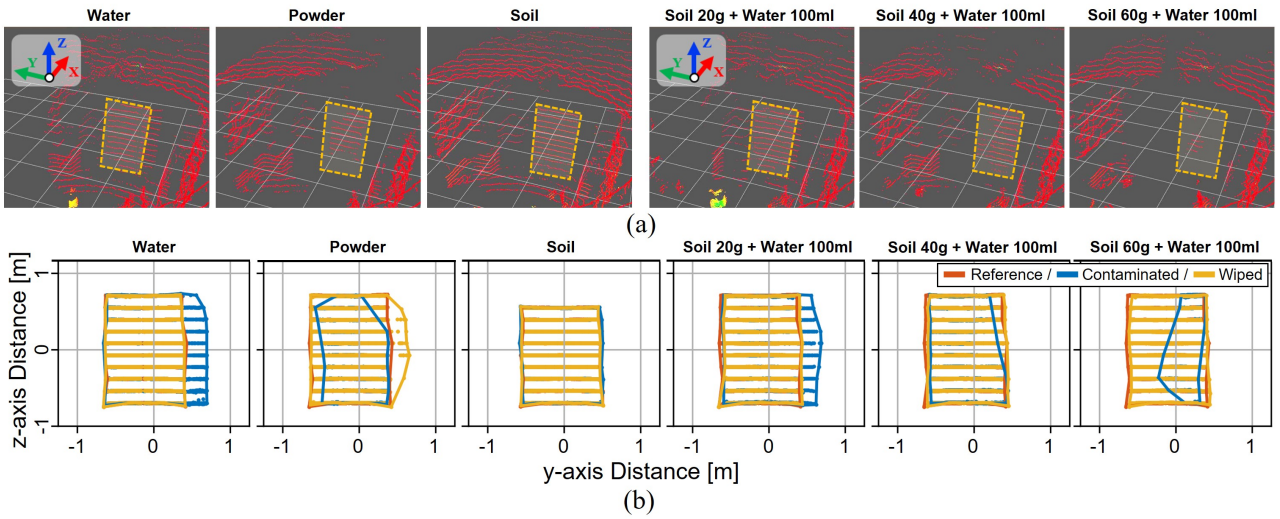

Fig. 9. Contaminated environment protection experiments. (a) Pointcloud data graph for different contamination. (b) Projection graph of pointcloud data and concave hull of projected data.

TABLE I
PROTECTION EXPERIMENT RESULTS

Experiment Case		Ref.	Cont.	Clea.	Loss	Rec.
Water	#	2553	2758	2485	-8.0%	97.3%
	I	58.502	37.573	47.062	35.8%	80.4%
Powder	#	2553	1559	2615	38.9%	97.6%
	I	58.502	16.496	42.715	71.8%	73.0%
Soil	#	2355	2368	2342	-0.6%	99.4%
	I	64.138	37.270	42.943	41.9%	67.0%
Soil 20g + water 100ml	#	2553	2537	2542	0.6%	99.6%
	I	58.502	29.814	45.328	49.0%	77.5%
Soil 40g + water 100ml	#	2553	1820	2591	28.7%	98.5%
	I	58.502	42.140	42.678	28.0%	73.0%
Soil 60g + water 100ml	#	2553	399	2570	84.4%	99.3%
	I	58.502	9.917	43.257	83.0%	73.9%

and I in Table I mean the numbers of pointcloud and average intensity. Ref., Cont., and Clea. indicate the reference, after contaminated, and after cleaned. Loss refers to the ratio of data lost due to contamination compared to the reference, and Rec. refers to the degree of data restored compared to the reference after cleaning. In the case of water and soil, there were cases where more pointclouds were detected than the reference due to data distortion. However, in most cases, the number and intensity of pointclouds decreased due to contamination. In all experimental cases, the number of pointclouds restored more than 97% of the reference data after cleaned. When the front of the sensor is contaminated with water, the rectangular shape of the data appears distorted. After being cleaned, the rectangular shape of the data was restored, and the number of pointclouds and average intensity were restored to the 97.3% and 80.4%. Even when the front of the sensor was contaminated with soil, an increase in the number of pointclouds and a decrease in average intensity were observed, and cleaning of the module restored them to the 99.4% and 67%. Furthermore, even in the case of high-concentration mud (Soil $60g$ + water $100ml$) where 84.4% of the pointcloud was lost, 99.3% of the data could be restored after being cleaned. In conclusion, as a result of conducting a cleaning experiment for contamination situations, the changes in the number of pointcloud and average intensity could be restored as the reference state after cleaning with the sensor protection module.

V. CONCLUSION

In this study, a protection module for LiDAR sensors used for outdoor unmanned vehicles was developed. To solve the inefficiency of the conventional LiDAR sensor protection devices, we theoretically analyzed the wiping motion of a human finger and derived that it is more efficient cleaning than the translational wiping motion. The water wiping experiment proved that the finger wiping motion had 35% better cleaning performance than the translational wiper method and matched the theoretical analysis's tendency. Through this, the protection module for LiDAR sensors that applied the wiping motion of a human finger was manufactured.

Experimental results confirmed that there was almost no distortion in using a rotating acrylic cover with a thickness of $2mm$, as the average error in the distance to the detecting target was up to 0.46%. A contamination environment protection experiment was conducted for water, powder, soil, and mud. As a result, it was proven that the change in pointcloud number and intensity reduction of sensor data due to contamination could be restored over 97% and 67% after cleaning. In summary, by imitating the wiping motion of a human finger, we have successfully developed a protection module for the LiDAR sensor of an outdoor unmanned vehicle that has excellent cleaning performance and efficiency and does not degrade the sensor performance.

REFERENCES

[1] G. P. Cruz Júnior, A. M. C. Rezende, V. R. F. Miranda, R. Fernandes, H. Azpúrua, A. A. Neto, G. Pessin, and G. M. Freitas, "EKF-LOAM: An adaptive fusion of LiDAR SLAM with wheel odometry and inertial data for confined spaces with few geometric features," *IEEE Trans. Autom. Sci. Eng.*, vol. 19, no. 3, pp. 1458–1471, Jul. 2022.

[2] Y. Su, T. Wang, S. Shao, C. Yao, and Z. Wang, "GR-LOAM: LiDAR-based sensor fusion SLAM for ground robots on complex terrain," *Rob. Auton. Syst.*, vol. 140, p. 103759, Jun. 2021.

[3] T. Guan, D. Kothandaraman, R. Chandra, A. J. Sathyamoorthy, K. Weerakoon, and D. Manocha, "GA-Nav: Efficient terrain segmentation for robot navigation in unstructured outdoor environments," *IEEE Robotics and Automation Letters*, vol. 7, no. 3, pp. 8138–8145, Jul. 2022.

[4] J. Li, H. Qin, J. Wang, and J. Li, "OpenStreetMap-Based autonomous navigation for the four Wheel-Legged robot via 3D-Lidar and CCD camera," *IEEE Trans. Ind. Electron.*, vol. 69, no. 3, pp. 2708–2717, Mar. 2022.

[5] X. Chen, D. Liu, J. Luo, T. Chen, G. Zhang, X. Rong, and Y. Li, "Realization of indoor and outdoor localization and navigation for quadruped robots," *Procedia Comput. Sci.*, vol. 209, pp. 84–92, Jan. 2022.

[6] D. Wisth, M. Camurri, and M. Fallon, "VILENS: Visual, inertial, lidar, and leg odometry for All-Terrain legged robots," *IEEE Trans. Rob.*, vol. 39, no. 1, pp. 309–326, Feb. 2023.

[7] Y.-C. Lin, Y.-T. Cheng, T. Zhou, R. Ravi, S. M. Hasheminasab, J. E. Flatt, C. Troy, and A. Habib, "Evaluation of UAV LiDAR for mapping coastal environments," *Remote Sensing*, vol. 11, no. 24, p. 2893, Dec. 2019.

[8] J. Sandino, F. Maire, P. Caccetta, C. Sanderson, and F. Gonzalez, "Drone-Based autonomous motion planning system for outdoor environments under object detection uncertainty," *Remote Sensing*, vol. 13, no. 21, p. 4481, Nov. 2021.

[9] M. Petrlík, T. Krajník, and M. Saska, "LIDAR-based stabilization, navigation and localization for UAVs operating in dark indoor environments," in *2021 International Conference on Unmanned Aircraft Systems (ICUAS)*. IEEE, Jun. 2021, pp. 243–251.

[10] H. Jung and I.-H. Lee, "Performance analysis of Millimeter-Wave UAV swarm networks under blockage effects," *Sensors*, vol. 20, no. 16, Aug. 2020.

[11] B. Schlager, T. Goelles, S. Muckenhuber, and D. Watzenig, "Contaminations on lidar sensor covers: Performance degradation including fault detection and modeling as potential applications," *IEEE Open Journal of Intelligent Transportation Systems*, vol. 3, pp. 738–747, 2022.

[12] M. Trierweiler, P. Caldelas, G. Gröninger, T. Peterseim, and C. Neumann, "Influence of sensor blockage on automotive LiDAR systems," in *2019 IEEE SENSORS*. IEEE, Oct. 2019, pp. 1–4.

[13] W. Kral and S. Dalpez, "Modular sensor cleaning system for autonomous driving," *ATZ worldwide*, vol. 120, no. 11, pp. 56–59, Nov. 2018.

[14] K. Göktürk and A. Jönsson, "Developing a Resource-Efficient sensor cleaning system for autonomous heavy vehicles," Ph.D. dissertation, 2019.

[15] "Waymo's method of cleaning its self-driving cars' sensors is delightful," [Accessed 18-4-2017]. [Online]. Available: https://digg.com/2017/waymo-clean-lidar

[16] M. S. P. Nogueira, "Glass cover with self-cleaning surface by coatings for automotive applications," Ph.D. dissertation, 2017.

[17] S. Son, W. Lee, H. Jung, J. Lee, C. Kim, H. Lee, S. Cho, J. Jang, M. Lee, and H.-C. Ryu, "Experimental analysis of various blockage performance for LiDAR sensor cleaning evaluation," *Sensors*, vol. 23, no. 5, Mar. 2023.

[18] A. Montanaro, L. Allocca, G. Maccariello, E. Frosina, L. Romagnuolo, and A. Senatore, "Experimental analysis of a water spray for the sensors cleaning at different injection pressures," in *2021 IEEE International Workshop on Metrology for Automotive (MetroAutomotive)*. IEEE, 2021, pp. 121–124.

[19] N. Pronk, B. Fildes, M. Regan, M. Lenné, N. Truedsson, and T. Olsson, "Windscreens and safety: A review," *Monash University Accident Research Centre Reports*, no. 183, p. 76, 2001.

[20] M. J. Allen, "Windscreen dirt and surface damage effects," *Clin. Exp. Optom.*, vol. 58, no. 5, pp. 180–189, May 1975.

[21] D. Kim and D. Yun, "A study on the effect of fingerprints in a wet system," *Scientific Reports*, vol. 9, no. 1, p. 16554, 2019.

[22] D. Kim, J. Yang, and D. Yun, "Anthropomorphic robot hand using the principle of sweat and fingerprints of human hands," in *2023 IEEE International Conference on Robotics and Automation (ICRA)*. IEEE, May 2023, pp. 10 289–10 295.

[23] J. S. Rowlinson and B. Widom, *Molecular Theory of Capillarity*. Courier Corporation, Apr. 2013.